Atmos. Chem. Phys. Discuss., doi:10.5194/acp-2016-862, 2016
Manuscript under review for journal Atmos. Chem. Phys.
Published: 30 September 2016

Atmospheric Chemistry and Physics Discussions

Arctic Regional Methane Fluxes by Ecotope as Derived Using Eddy Covariance from a Low Flying Aircraft

David S. Sayres[1], Ron Dobosy[2,3], Claire Healy[4], Ed Dumas[2,3], John Kochendorfer[2], Jason Munster[1], Jordan Wilkerson[5], Bruce Baker[2], and James G. Anderson[1,4,5]

[1]Paulson School of Engineering and Applied Sciences, Harvard University, 12 Oxford Street, Cambridge, MA 02138
[2]Atmospheric Turbulence and Diffusion Division, NOAA/ARL, Oak Ridge, TN
[3]Oak Ridge Associated Universities (ORAU), Oak Ridge, TN
[4]Department of Earth and Planetary Sciences, Harvard University, 12 Oxford Street, Cambridge, MA 02138
[5]Department of Chemistry and Chemical Biology, Harvard University, 12 Oxford Street, Cambridge, MA 02138

Correspondence to: David Sayres (sayres@huarp.harvard.edu)

Abstract. The Arctic terrestrial and subsea permafrost region contains approximately 30% of the global carbon stock and therefore understanding Arctic methane emissions and how they might change with a changing climate is important for quantifying the global methane budget and understanding its growth in the atmosphere. Here we present measurements from a new *in situ* flux observation system designed for use on a small, low-flying aircraft that was deployed over the North Slope of Alaska during August of 2013. The system combines a small methane instrument based on Integrated Cavity Output Spectroscopy (ICOS) with an air turbulence probe to calculate methane fluxes based on eddy covariance. We group surface fluxes by land class using a map based on LandSat Thematic Mapper (TM) 30 meter resolution data. We find that wet sedge areas dominate the methane fluxes with a mean flux of 2.1 $\mu g \cdot m^{-2} \cdot s^{-1}$ during the first part of August, with methane emissions from the Sagavanirktok river being the second highest at almost 1 $\mu g \cdot m^{-2} \cdot s^{-1}$. During the second half of August, after soil temperatures had cooled by 7 °C, methane emissions fell to between 0 and 0.5 $\mu g \cdot m^{-2} \cdot s^{-1}$ for all areas measured. We compare the aircraft measurements with an eddy covariance flux tower located in a wet sedge area and show that the two measurements agree quantitatively when the footprints of both overlap. However, fluxes from sedge vary at times by a factor of two or more even within a few kilometers of the tower demonstrating the importance of making regional measurements to map out methane emission spatial heterogeneity. Aircraft measurements of surface flux can play an important role in bridging the gap between ground-based measurements and regional measurements from remote sensing instruments and models.

1 Introduction

Methane is the third most important greenhouse gas after water vapor and carbon dioxide and its concentration in the atmosphere has increased from a pre-industrial value of 0.7 parts per million by volume (ppmv) to its current value of approximately 1.85 ppmv. Methane sources are varied, with major contributors being anthropogenic (including fossil and agricultural) as well as natural. Often multiple sources occur in the same vicinity, for example emissions from gas wells collocated with agricultural fields or pasture for grazing livestock. In the past few years there have been increased efforts to understand how methane emis-

Atmos. Chem. Phys. Discuss., doi:10.5194/acp-2016-862, 2016
Manuscript under review for journal Atmos. Chem. Phys.
Published: 30 September 2016

Atmospheric Chemistry and Physics Discussions

sions, as well as carbon dioxide, might change from the Arctic region in response to warmer temperatures (Yvon-Durocher et al., 2014; Sturtevant et al., 2012; Sturtevant and Oechel, 2013; Walter et al., 2007b, and references therein). For example, temperatures in the Alaskan North Slope have increased 0.6 °C per decade for the last 30 years. Likewise, in that same time period the minimum extent of Arctic sea ice at the end of the summer has decreased from 8 million km^2 to 5 million km^2. Late summer sea ice extent until this past century was 10 million $\pm$ 1 million km^2 over the past 1500 years (Kinnard et al., 2011). Global methane concentrations have also varied during this time period, with atmospheric increases slowing down in the 1990s, leveling off in the early part of the 21st century and then increasing again since 2007 with concentrations reaching 1.8 ppmv in 2010 based on several surface based observation networks (Kirschke et al., 2013). It has been postulated that the increase could be from Arctic wetlands (Koven et al., 2011; Walter et al., 2007b). A brief look at the carbon stock in the Arctic reveals why it has garnered so much attention. The Arctic permafrost region contains between 1330 and 1580 Pg of carbon in the surface layer (0-3 meters depth), Yedoma region and rivers. An additional quantity is contained in deeper deposits and subsea permafrost (Tarnocai et al., 2009). Arctic carbon stock represents about a third of the total global surface carbon pool and increases to 50% when accounting for the deeper soils (Schuur et al., 2015). As the climate continues to warm, this carbon is vulnerable to thaw and decomposition by microbes, potentially leading to large increases in methane and carbon dioxide emissions. Particularly important are organic carbon stocks in permafrost reduced anaerobically to methane, as the latter has a warming potential more than twenty times larger than carbon dioxide on a 100-year time scale which increases over shorter time periods (Boucher et al., 2009). The release of methane and carbon dioxide from northern wetlands and ocean clathrates in response to a warming Arctic exhibits strong evidence in the paleoclimate record (Zachos et al., 2008; Whiticar and Schaefer, 2007). It is also supported by current observations of methane release from thermokarst lakes formed from melting Arctic permafrost each spring and summer (Sepulveda-Jauregui et al., 2015; Walter et al., 2007b; Bastviken et al., 2004; Casper et al., 2000), from ebullition from deep sea sediments (Shakhova et al., 2014; Reagan et al., 2011; Damm et al., 2010), and from airborne campaigns (Wofsy, 2011; Chang et al., 2014).

The North Slope of Alaska is covered by several different land classes though dominated by permafrost and the interior is mostly accessible only by airplane or helicopter with the exception of Prudhoe Bay which sits at the end of the Dalton Highway (Rt. 11) which extends from Fairbanks to Prudhoe Bay. The lack of infrastructure, especially roads, makes continuous ground based measurements difficult except near the major settlements, which in turn makes regional bottom-up estimates of carbon flux uncertain owing to the sparsity of data. At the same time top-down estimates based on inversion modeling rely on some knowledge of flux sources on the ground and lack the spacial resolution to discriminate which sources are dominating the emissions in areas like the North Slope where there are a multitude of broad-scale emitters and point sources. Airborne measurements, especially from low flying aircraft, have the potential to bridge the scale gap between process level studies on the ground and large scale regional estimates from remote sensing data or inversion modeling of concentration profiles. Flux measurements from low-flying aircraft coordinated with surface measurements allow for the detailed surface flux measurements to be extended to the larger regional scale by mapping the heterogeneity in the fluxes over these larger areas.

Eddy covariance is a direct way to determine the exchange of mass, momentum, and energy between the atmosphere and the surface. The covariance between turbulent wind and concentration is calculated directly from the individual variances from the

Atmos. Chem. Phys. Discuss., doi:10.5194/acp-2016-862, 2016
Manuscript under review for journal Atmos. Chem. Phys.
Published: 30 September 2016

Atmospheric Chemistry and Physics Discussions

mean and as wind and concentration measurements can be routinely obtained, eddy covariance from the ground or towers is widely represented in the literature as a way of obtaining the flux of a quantity between the surface and atmosphere. Obtaining eddy covariance measurements from a moving aircraft presents some unique challenges including accurately measuring turbulent wind velocity relative to the ground and measuring concentration at high data rate (∼10 Hz for a slow moving aircraft). Even with these, in order for the flux from the aircraft to be a good proxy for a measurement taken at the surface, it needs to be sampled close to the ground, with the exact distance varying depending on boundary layer height, turbulence, and the footprint size of interest. Even with these difficulties, several groups have successfully measured carbon dioxide and heat flux from low flying aircraft in the Arctic (Zulueta et al., 2011; Oechel et al., 2000, 1998; Gioli et al., 2004), Europe (Bange et al., 2007; Vellinga et al., 2010; Hutjes et al., 2010; Gioli et al., 2006), Asia (Metzger et al., 2013), and continental US (Kirby et al., 2008; LeMone et al., 2003; Avissar et al., 2009).

Here we present *in situ* methane fluxes taken during the summer of 2013 in the North Slope of Alaska. Using two different methods for calculating flux we show that airborne flux measurements can compare with tower measurements when attention is paid to properly overlapping the footprints of the airplane and the tower. We also derive fluxes from several different land classes and compare with estimates using more traditional ground based techniques.

2 Methods

To measure methane emissions over large areas of the North Slope, the Flux Observations of Carbon from an Airborne Laboratory (FOCAL) system was flown during August, 2013 out of Deadhorse Airport, Prudhoe Bay, AK. FOCAL, pictured in Fig. 1 flying near the NOAA Atmospheric Turbulence and Diffusion Division (NOAA/ATDD) flux tower, consisted of three main parts: the aircraft, a Diamond DA-42 from Aurora Flight Sciences, a turbulence probe, the Best Airborne Turbulence (BAT) Probe from NOAA/ATDD, and a fast methane and water instrument from the Anderson Group at Harvard University. Data presented in the results section was obtained during six flights between August 13 and August 28 (Fig. 2 and Table 1). During three of these flights the aircraft made repeated passes near the NOAA/ATDD tower that was set up for comparisons. The other three flights were flown as grid patterns over large regional areas (50x50 km^2) to better sample the heterogeneity of different land types over a large region. These flights consisted of both profiles from the bottom of the boundary layer (∼5-10 m) up to ∼1500 m altitude and long transects (∼50 km) at low altitudes (< 25 m) that are used to access surface flux using eddy covariance.

2.1 FOCAL instrumentation

The airborne methane flux calculations rely on having fast (10 Hz) measurements of both turbulent wind velocity and dry-air mixing ratio with the two quantities being coordinated in time and space to better than the measurement time, which in this case is 20 milliseconds. NOAA/ATDD developed the BAT probe in the 1990s as a pioneering low-cost solution for mobile atmospheric turbulence measurements (Crawford et al., 1996, 1993; Crawford and Dobosy, 1992). The BAT probe consists of a hemisphere, 15.5-cm in diameter, with nine pressure ports located at selected positions on the probe head. The vertical

Atmos. Chem. Phys. Discuss., doi:10.5194/acp-2016-862, 2016
Manuscript under review for journal Atmos. Chem. Phys.
Published: 30 September 2016

Atmospheric Chemistry and Physics Discussions

and horizontal pairs of ports measure the differential pressure between them to calculate the angle of attack and side slip, respectively. Static pressure is taken as the average of the pressures measured at the four diagonal pressure ports correcting for the attack and sideslip angles. Dynamic pressure is measured as the difference between the pressure measured at the center hole and the static pressure, again correcting for small errors as the angles of attack and sideslip are not truly zero. These pressure measurements are combined with a known model for flow over a hemisphere to determine three dimensional wind direction and speed relative to the probe. In order to get the velocity of the probe relative the ground a GPS/INS system located near the center of gravity (CG) of the aircraft and two GPS antennas, one located on the BAT probe and the other located on top of the main cabin, provide for the movement of the BAT probe relative to the aircraft and the aircraft relative to the Earth's surface (Crawford and Dobosy, 1997, 1992). Fluxes of trace gases are covariances between turbulent winds and fluctuations in gas concentration. The BAT probe was designed to accurately measure turbulent winds from a moving aircraft and, using accelerometers and GPS/INS, relate those winds to the surface. The BAT probe digitizes samples at 1600 Hz for low-pass filtering and subsampling at 50 Hz to suppress aliasing. The wind measurements are synchronized with the 50 Hz signal from the GPS/INS system. In calculating fluxes, the 10 Hz data from the spectrometers discussed below are interpolated to 50 Hz and synchronized with the data from the BAT probe.

The methane instrument draws air from an inlet located 8 cm aft of the BAT probe turbulence measurements. Flow of air through the axis is controlled by a dry scroll pump located in the back of the aircraft. Air from the inlet passes through 1.25 cm diameter tubes into the nose and forward luggage bay sections of the aircraft. The pressure of the air is controlled by a proportional solenoid valve and a pressure control board that uses pressure measured at the detection axis to feed back on the valve orifice position. The actual detection axis is located in the port side forward luggage bay. The methane instrument uses Integrated Cavity Output Spectroscopy (ICOS) to measure CH_4, H_2O and N_2O (Witinski et al., 2011). The ICOS instrument uses a high finesse optical cavity composed of two high-reflectivity mirrors (R = 0.9996) to trap laser light for a period on the order of 2 µs producing effective path lengths 10^3 times the mirror separation. For the fast methane sensor used in this deployment a small ICOS cell (25 cm in length; 5 cm diameter mirrors) was built that combines the sensitivity and stability of ICOS with a small sample volume to attain high flush rates (17 Hz). Using the wavelength region around 1292 cm^{-1} (7.74 µm), measurements of methane achieved a precision of 7 ppbv ($1-\sigma$, $1-\mathrm{s}$). Due to the high variability of water in the troposphere, water vapor measurements are required with any trace gas measurements in order to quantify dilution effects caused by changes in water vapor content as well as changes to spectroscopic line broadening. Well defined absorption features of water vapor and its isotopologues as well as nitrous oxide are obtained in the same sweep of the laser, therefore the same instrument provides simultaneous measurements of nitrous oxide and water vapor along with methane. This technique provided extremely high signal to noise observations as well as a robust measurement in flight and has been the basis for several ICOS flight instruments built by this group (Witinski et al., 2011; Sayres et al., 2009; Engel et al., 2006; Paul et al., 2001). Periodic calibration in flight using calibrated gas cylinders were used to track drift over the course of the flight and from flight to flight. There were several other small instruments that augmented FOCAL's capabilities: a radar altimeter, for height above ground which is essential for accurate footprint calculations, and a visible camera, which provided a visual record of the terrain directly under the aircraft used to check the accuracy of remotely sensed products that are used for primary landscape classification.

Atmos. Chem. Phys. Discuss., doi:10.5194/acp-2016-862, 2016
Manuscript under review for journal Atmos. Chem. Phys.
Published: 30 September 2016

Atmospheric Chemistry and Physics Discussions

Aurora Flight Sciences' version of the DA-42, named the Centaur, is a twin-engine aircraft, and has several characteristics that make it an ideal platform for the work discussed here. Due to the twin engine configuration, the entire center fuselage is available for instrumentation and sampling. The Centaur is electrically and structurally well-adapted for carrying a sophisticated scientific payload, having ample spare power from its two alternators and ideally located hard points for the probe and the spectroscopic equipment. Finally, once fixed costs (e.g. aircraft access, instrument integration and certification) have been accounted for, the operating cost of the Centaur are just $1500 per day and $600 per flight hour - a substantial savings compared to many other scientific platforms.

2.2 Turbulence measurements

Eddy covariance is a direct way to determine the exchange of mass, momentum, and energy between the atmosphere and the surface. Since the observed flux is assumed to represent the exchange at the surface, the airplane is flown as low as is safely possible, typically below 30 m (Mahrt, 1998). Flux measurements from fixed surface sites, important complements to the airborne measurements, provide extended temporal coverage at selected locations as well as validation of the airborne flux measurements. The covariance of the dry-air mixing ratio of these gases (Webb et al., 1980; Gu et al., 2012) with the turbulent vertical wind component determines the flux as shown in Eq. (1) where the bar represents the average which defines the base state, ρ_a is the dry air density, w' is the departure of the wind from the base state, and c' is the analogous departure of the methane mixing ratio of dry air.

$$F = \overline{(\rho_a w')c'} \tag{1}$$

Unlike a stationary tower, measuring the turbulent vertical wind component from an airplane requires finding the small (vector) sum of the airspeed and the ground speed, two large, nearly canceling vectors. Since both vectors fluctuate rapidly and independently, many independent measurements must be made with precise synchrony at high accuracy and sample rate. Since turbulent fluctuations can be less than 0.1 m/s, the two large velocities must each be accurate within 0.1 m/s. Four samples define the minimum effectively resolvable turbulent eddy size, about 5 m at 60 m/s.

The Centaur uses a small Inertial Navigation System integrated with a GPS (GPS/INS) to report its ground-speed vector over the surface as well as its roll, pitch, and heading, all at 20 Hz. The low-frequency component of the Centaur's velocity is filtered to 1 Hz and extrapolated to the probe's location to mix with the high-frequency component measured directly at the probe. The airspeed vector (airflow relative to the probe) is determined from the distribution of induced pressure over the BAT probe's hemispherical surface. One static pressure and three differential pressures are taken over nine ports. From these four pressure measurements plus temperature come the five relative-flow parameters: ambient pressure, ambient temperature, and three components of the airflow relative to the probe. The dominant airflow component is along the airplane's longitudinal axis, approximately equal to the airplane's true airspeed.

Atmos. Chem. Phys. Discuss., doi:10.5194/acp-2016-862, 2016
Manuscript under review for journal Atmos. Chem. Phys.
Published: 30 September 2016

Atmospheric Chemistry and Physics Discussions

2.3 Methane Flux Measurements

2.3.1 Running Flux Method

The running flux method (RFM) (e.g. LeMone et al., 2003) is commonly used to analyze airborne fluxes. The RFM calculates the mean flux over a contiguous integration length (e.g., 3 km). As opposed to a stationary tower, which averages in time, the aircraft is moving over the landscape, so that fluxes are more appropriately averages over distance. Here we use the same notation as Crawford et al. (1993)

$$F = \frac{\sum_{k=1}^{N} (\rho_d w)_k^{'} c_k^{'} V_k}{\sum_{k=1}^{N} V_k} \tag{2}$$

where ρ_a, *w'*, and *c'* are defined as in Eq. (1) and *V* is the airspeed of the aircraft. The sum is over *N* consecutive samples and the denominator is the spacial averaging length. For the analysis presented here we use a 3 km window that is moved by 1 km increments so that, unlike the normal practice with tower data, there is overlap between adjacent calculated fluxes to provide smoothed interpolation. The RFM quantitatively describes the relation between measured flux and underlying surface features of scales comparable to the averaging length or larger. This method works well as shown by LeMone et al. (2003) who found a 4 km moving average on the US Great Plains to be an appropriate compromise between uncertainty in flux estimation and resolution of landscape-scale heterogeneity. In the Arctic in 2013, the much smaller mixed layer depth gave rise to smaller turbulence scales. Ogive analysis of the frequency distribution showed 3 km to suffice as the integration distance (Berger et al., 2001). However, heterogeneity in the resulting flux estimates was large and repeated flight segments gave variable results likely due to changes in winds and sampling footprints and the scale of the underlying surface features being smaller than the integration length. Nevertheless, there was good agreement between methane fluxes calculated by the RFM using 3 km integration centered near the tower location and fluxes computed directly from the tower measurements (see sec. 3.1). However, given the small scale heterogeneity of surface features on the North Slope using the RMF limits the ability to separate out flux contribution from individual surface types.

2.3.2 Flux Fragment Method

The flux fragment method (FFM) (Kirby et al., 2008) uses a conditional sampling scheme whereby flux is compiled from many τ-second 'fragments' of flux of a quantity, such as methane, along a transect given by

$$f_i = \delta t \sum_{k=1}^{n\tau} [(\rho_d w)_k^{'} c_k^{'} V_k]_i \tag{3}$$

$$L_i = \delta t \sum_{k=1}^{n\tau} [V_k]_i \tag{4}$$

where *n* is the number of samples per second, δt is the sample interval, and everything else is defined as in Eq. (2) except that instead of summing over a large distance, such as 3 km, the sum is only over a few samples. In the case of the data presented here the fragments are 1 second sums ($\tau = 1$second) of approximately 60 m length. The fragments, labeled f_i, do not constitute

Atmos. Chem. Phys. Discuss., doi:10.5194/acp-2016-862, 2016
Manuscript under review for journal Atmos. Chem. Phys.
Published: 30 September 2016

a Reynolds average individually meaning an individual fragment is not long enough to average over all the frequencies that are important for eddy transport. Instead, they provide a meaningful flux estimate only in aggregate. Fragments can be grouped, for example, by surface class, determined from footprint estimation (Fig. 3). The sum over each group divided by the total length of all fragments in the group provides the mean flux from the associated surface class as given by

$$F_S = \frac{\sum_{i \in S} f_i}{\sum_{i \in S} L_i} \tag{5}$$

The FFM is most appropriate in a region that is heterogeneous on small scales (100 m to 3 km), but relatively homogeneous on large scales such that many instances of the surface class, or other classification used to group the fragments, are sampled during the flight (See Kirby et al. (2008) for the full description of the method). Initial assessments of the data presented here indicate that the FFM is well suited for application to the North Slope, where Arctic tundra is interspersed with thermokarst lakes, bogs, fens and bare ground. First, land-cover data is classified using a current land-cover image at 100 m resolution or better (e.g. LandSat). We use this to establish transects at altitudes typically 10 m to 30 m above ground; low as safely possible. These are flown repeatedly and coordinated with eddy-covariance towers for validation and temporal continuity. The base state is then defined, representing in principle the deterministic (non-turbulent) mesoscale component of the flow. Flux fragments are calculated using 1 s sums of squares and cross products of departures from the base state. Finally, a footprint model is applied to estimate the level of influence of each surface type on each fragment which allows the fragments to be grouped by type having a predetermined probability of coming from a single surface type (see sec. 3.2 for examples of how FFM is used to interpret these data). We use the parameterization scheme described in Kljun et al. (2004) which uses a backward Lagrangian model (Kljun et al., 2002) for a range of heights, stability measures and other turbulence quantities that are measured from the aircraft. The flux estimate for each land surface type is the sum of the fragments in the associated group divided by their accumulated length. The number of fragments necessary to provide a robust result can be determined by bootstrap resampling (Kirby et al., 2008). For the data presented here 3 km or ∼50 fragments suffice.

2.4 Land Surface Classification

The land surface on the North Slope can be divided into different classes based on dominant plant species, topography, soil content, and soil moisture. The North Slope Science Initiative (NSSI) has identified 24 classes based on Landsat Thematic Mapper (TM) 30 meter resolution land cover maps in conjunction with field surveys (Initiative, 2013). These classifications, assigned based on remotely sensed data, are good proxies for properties that have been shown to be primary drivers of methane production and emission such as water table height, soil content, and emission pathways such as sedge roots. The areas flown over by FOCAL were dominated by a mixture of wet sedge, mesic sedge - dwarf shrub, fresh water marsh, tussock tundra, and open water consisting of both lakes and rivers (Fig. 2). Open water is visible from the air and includes lakes of various sizes and origin and rivers but for this analysis excludes coastal waters. By definition in the tussock-tundra land class, shrubs more than 20 cm tall occupy less than 25% of the surface, and tussocks occupy more than 35%. The sites are cold, poorly drained and underlain by mesic to wet, silty to sandy mineral soils with a shallow surface organic layer surrounding the tussocks. Wet sedge sites are defined as those with sedge species accounting for more than 25% of the cover and Sphagnum for less than 25%.

Atmos. Chem. Phys. Discuss., doi:10.5194/acp-2016-862, 2016
Manuscript under review for journal Atmos. Chem. Phys.
Published: 30 September 2016

Atmospheric Chemistry and Physics Discussions

Soils range from acidic to non-acidic, are saturated during the summer, and typically have an organic layer over silt or sand. Mesic sedge - dwarf shrub has shrubs less than 25 cm tall covering more than 25% of the area and sedge cover is also more than 25%. Soil surface is generally mesic, but sometimes wet and is calcareous to acidic. The fresh water marshes (FWM) are semi-permanently flooded, but some have seasonal flooding, and the water depth typically exceeds 10 cm. Soils are muck or mineral, and the water can be nutrient-rich.

We use land types, as defined by a remote measurement, as opposed to soil properties such as moisture, organic carbon content, temperature, etc. as the remotely based definition is most appropriate to comparing to larger regional scale models and satellites. It should be noted therefore that land type here is a proxy for general classifications of areas with different soil moisture and other properties which are likely the primary drivers of differences in methane emissions, though certain plants such as sedge have been shown to act as conduits for direct methane release from the soil to the atmosphere through the plants vascular system (Olefeldt et al., 2013).

2.5 Tower Measurements

Starting a few weeks before the flight campaign and throughout the month of August, a small portable flux tower was setup at 70.08545° North latitude, 148.57016° West longitude, just south of Prudhoe Bay off the Dalton Highway. During that time the tower recorded CO_2 flux, CH_4 flux, latent heat flux, sensible heat flux, air temperature, and incoming radiation. Soil temperature probes were also used to record soil temperature at 2-cm, 5-cm, 10-cm, and 20-cm depth at three different locations around the tower. The tower was situated in an area dominated by sedge grass, and the surrounding area's water table was frequently near the surface such that the surroundings were puddled and muddy, especially in late August 2013. On the NSSI map the area is labeled as wet sedge. Since low light and convective conditions are common on the North Slope of Alaska, data collected during still conditions do not provide reliable eddy covariance flux measurements. Consequently data where the standard deviation of the vertical wind speed was less than 0.1 $\mathrm{m/s}$ were removed from the final data set.

3 Results and discussion

3.1 Comparison between aircraft and tower fluxes

On three separate flights FOCAL flew along a transect near the flux tower affording the opportunity for direct comparison between methane flux measured by an eddy covariance tower and by eddy covariance from a moving aircraft. It also allowed for comparisons of methane flux from the ecotope of the tower, in this case wet sedge, with methane flux from sedge averaged over the 50 km transect of the aircraft to look at spatial heterogeneity in the flux from this land type. We present these comparisons with varying levels of footprint overlap and show quantitatively how proper overlap affects the agreement between the tower and aircraft data. On August 13, 25, and 27 the aircraft flew multiple transects in a nominally East-West direction near the tower (Fig. 2). Based on the forecast wind direction, the tracks were slightly south of the tower on August 13 and 25 and north of the tower on August 27. Figure 4 shows 30-minute mean methane fluxes as measured by the flux tower from August 12

Atmos. Chem. Phys. Discuss., doi:10.5194/acp-2016-862, 2016
Manuscript under review for journal Atmos. Chem. Phys.
Published: 30 September 2016

Atmospheric Chemistry and Physics Discussions

to August 29. Fluxes at the tower site roughly correlate with soil temperature with the first half of August showing most 30-minute mean methane fluxes ranging from 1 to 2.5 $\mu g \cdot m^{-2} \cdot s^{-1}$, when soil temperatures at a depth of 10 cm were 10-14 °C, and the second half of August showing most 30-minute mean methane fluxes ranging from 0.5 to 1.3 $\mu g \cdot m^{-2} \cdot s^{-1}$, when soil temperatures at a depth of 10 cm were 3-6 °C. The observed temperature dependence is consistent with previous studies (e.g. Yvon-Durocher et al., 2014). Aircraft methane fluxes for comparison with the tower were calculated by finding the closest point along each leg of the flight to the flux tower and taking a 3-km RFM centered at that point. The mean of the RFM fluxes for each flight are plotted over the 30-minute fluxes from the tower in Fig. 4 (orange circles). Also shown are the fluxes associated with four different land types sampled during the flights using the FFM to calculate flux. The 95% confidence intervals, using bootstrapping, for fluxes derived using RFM and FFM are shown in the three insets. Agreement between the aircraft and tower on August 13 and 25 are within the confidence intervals of the data, though the aircraft measures significantly less methane flux than the tower on August 27. On August 13 the methane flux from wet sedge (red line), as derived using FFM, agrees very well with the magnitude of the flux measured by the tower, which sits on a sedge site. However, on August 25 the flux from sedge is lower than the tower measurements and on August 27 is also lower, though closer to the tower flux than the flux calculated by RFM near the tower.

The differences between the flux measured by the tower and aircraft can be explained by looking at the aircraft footprints for the three flights. Figure 5 shows footprints for selected fragments from each day. On both August 13 and 25 the dominant wind direction was from the North, and the parts of the footprint with the highest probability of influence on the flux fragments (maroon points in Fig. 5) are over sedge. On August 27 the aircraft flew North of the tower as the winds were primarily from the East. While the aircraft footprints did overlap the tower footprint, the highest probability of influence for the fragments (>80%) was from lakes North-West of the tower. Lakes have been shown to be sporadic hot spots of methane ebullition, but at least at the time of flight these lakes showed very low methane emissions. It is clear that even with flight plans that take into account forecast wind direction, careful attention to footprints must be taken when comparing different measurements. Most importantly though, is that when there is reasonable overlap between tower and aircraft footprints, the flux measurements from the aircraft agree with the tower measurements adding another level of validation to the aircraft data.

Though the tower site was situated on wet sedge, the agreement between averaging sedge sites along the approximately 50 km transect of the aircraft and just looking at the sedge in proximity to the tower varied considerably throughout the course of the mission. During the period of consistent warmth in the beginning part of August, methane emissions from sedge averaged over the whole domain of the aircraft flight track agreed with the tower measurements (Fig. 4, inset (a)). During the latter half of August, as both the soil and air temperatures cooled, likely due to decreased insolation, the tower consistently measured almost twice as much emission as the aircraft (Fig. 4, insets (b) and (c)). Using the RFM to calculate 3 km mean fluxes along the flight transect, which is dominated by sedge, the tower location stands out as a hot spot for methane emissions as shown in Fig. 6. Emissions from the tower region are twice as large as those from the rest of the flight track consistent with the tower measuring almost twice as much as sedge. Though not shown, latent heat flux showed a similar pattern to that of methane. While we have soil temperature and moisture measurements only near the tower, it is possible that the tower was in a locally wet or warm spot leading to larger methane emissions than westward of the tower. This underscores the importance of coordinating local

Atmos. Chem. Phys. Discuss., doi:10.5194/acp-2016-862, 2016
Manuscript under review for journal Atmos. Chem. Phys.
Published: 30 September 2016

measurements, such as with a tower, with larger scale measurements from an aircraft that can show the regional heterogeneity of methane fluxes associated with land classes that from remote measurements look the same.

3.2 Regional methane fluxes

During August, 2013 FOCAL measured methane flux from a variety of ecotopes across the North Slope. In order to distinguish the contribution to the total methane flux from individual land types, the data are filtered to only include flux fragments where 85% of the probability density comes from a single land class. Increasing this metric, increases the causal relationship between the calculated flux and a single land class, but reduces the number of footprints available for the analysis thus loosening the confidence interval. Varying this filter between 80% and 95% produces only a small effect on the quantification of flux from each land class. We find that 85% is a good compromise between singling out individual land classes while still retaining a large dataset. For the flight speed of the Centaur at low altitude and wind conditions during the flights, the footprint length for each 60-m fragment varied between 0.5 and 5 km, though the part of the footprint whose probability density of contributing more than 90% of the flux was only between 100 and 800 m. The above filter eliminates about half of the flux fragments from each flight. Of those, we limit the land classes to those where the total number of flux fragments is more than 50 fragments or an equivalent distance of 3 km. The flux fragments are summed and then divided by the total integration length for each land cover type (Fig. 7). Land cover type varies over the North Slope, so different flights sampled different types of terrain (see Table 1 and Fig. 2), with wet sedge being the most dominant and thus sampled on each flight. Other land cover classes such as bare ground, dwarf shrub, and low-tall willow were also observed but not with sufficient frequency to calculate a statistically significant flux. Prevalent near the tower site, which was sampled on August 13, 25, 27, were wet sedge, mesic sedge-dwarf shrub, some lakes, the Sagavanirktok (Sag) river, and fresh water marsh. Soil temperatures in mid-August varied by 1.5 ^{o}C with a mean soil temperature of 8 ^{o}C at 5 cm depth. By the end of August soil temperatures had dropped to a mean of 3 ^{o}C. Sedge showed the strongest correlation with soil temperature, with fluxes falling from 2.1 $\mu g \cdot m^{-2} \cdot s^{-1}$ on August 13th to less than 0.5 $\mu g \cdot m^{-2} \cdot s^{-1}$ by the end of August. This relationship held true for emissions from the Sag river with emissions falling from 1 $\mu g \cdot m^{-2} \cdot s^{-1}$ to near 0. Lakes showed no trend though it should be noted that the number of lakes sampled on August 13 was small as indicated by the large 95% confidence interval. While data on August 13 was sparse for the other land classes sampled, during the latter half of August emissions from fresh water marsh and tussock tundra were similar to those from lakes and sedge.

Airborne measurements made during August, 2013 are consistent with findings from other studies. Olefeldt et al. (2013) reported sites dominated by sedge and wet soils having methane emissions ranging from 0.46 to 1.6 $\mu g \cdot m^{-2} \cdot s^{-1}$ with a median value of 0.87 $\mu g \cdot m^{-2} \cdot s^{-1}$ across multiple permafrost sites. Other studies at single locations fall into this same range. For example, Harazono et al. (2006) measured methane fluxes from a wet sedge site in Happy Valley, AK during August of 1995 ranging from 0.38 to 1.5 $\mu g \cdot m^{-2} \cdot s^{-1}$ and Sturtevant and Oechel (2013) measured wet sedge near Barrow with emissions of 0.39 ± 0.03 $\mu g \cdot m^{-2} \cdot s^{-1}$ with short periods of higher emissions up to 1.1 $\mu g \cdot m^{-2} \cdot s^{-1}$. Emissions from mesic-sedge sites near the Sag river, though south of the areas measured by FOCAL, showed fluxes of 0.35 to 0.58 $\mu g \cdot m^{-2} \cdot s^{-1}$ in the first half of August falling to 0.12 to 0.23 $\mu g \cdot m^{-2} \cdot s^{-1}$ in the second half of August (Harazono et al., 2006).

Atmos. Chem. Phys. Discuss., doi:10.5194/acp-2016-862, 2016
Manuscript under review for journal Atmos. Chem. Phys.
Published: 30 September 2016

Atmospheric Chemistry and Physics Discussions

Emissions from lakes tend to be more variable than the land classes with measured emissions from individual lakes ranging from 0.25 to 6.3 $\mu g \cdot m^{-2} \cdot s^{-1}$ across various thermokarst and other lakes in the North Slope (Walter et al., 2007a; Sepulveda-Jauregui et al., 2015). These fluxes are reported as means over a year, so emission rates during short periods of time may be lower or higher for an individual lake. While FOCAL did not sample the same lakes as in the aforementioned studies, during the flights near the tower multiple passes over the same lakes allow emissions from individual lakes to be measured. On August 13, five lakes were sampled with sufficient frequency to produce a statistically significant flux ranging from 0 to 2.6 $\mu g \cdot m^{-2} \cdot s^{-1}$. On August 25 a single lake was measured with an emissions rate of 0.72 $\mu g \cdot m^{-2} \cdot s^{-1}$. On August 27 four lakes were measured with emissions ranging from 0.09 to 0.18 $\mu g \cdot m^{-2} \cdot s^{-1}$. These data are consistent with the rates measured by the above studies.

4 Conclusions

The FOCAL campaign during the summer of 2013 showed how methane fluxes could be successfully measured over large regions using airborne eddy covariance measurements from a small, low-flying aircraft. Comparing the airborne measurements to those of a tower showed that the data were quantitatively comparable when there was good overlap between the tower footprint and aircraft footprint. However, along the flight track local conditions dominated the flux especially in the transition season from summer to fall in late August. Comparing wet sedge at the tower site with wet sedge west of the tower showed a factor of two difference in methane emissions during the later half of August which underscores the importance of regional measurements as fluxes can have large dependence on spatial heterogeneity even over relatively short distances. During the middle of the summer fluxes from sedge were more homogeneous across the area flown.

Measurements of methane flux over the North Slope of Alaska in August showed a strong correlation with soil temperature consistent with previous studies. Wet sedge showed the highest persistent methane emissions with mean fluxes about 2 $\mu g \cdot m^{-2} \cdot s^{-1}$ in the first half of August falling to 0.2 $\mu g \cdot m^{-2} \cdot s^{-1}$ in the latter half of August. Emissions from the Sag river showed a similar trend, while other land surface classes were not sampled enough during the first half of August to provide a statistically significant sample. Individual lakes sampled near the tower showed a large range of emissions varying from near 0 to 2.6 $\mu g \cdot m^{-2} \cdot s^{-1}$ consistent with the range of lake emissions reported in the literature.

Aircraft measurements of surface flux can play an important role in bridging the gap between ground-based measurements and regional measurements based on inversion modeling or downwind-upwind differences. While airborne campaigns are generally more costly than ground based measurements, using small aircraft these costs can be minimized and for areas that are logistically challenging to access, such as the North Slope, airborne eddy covariance presents the easiest and least expensive way to directly measure surface fluxes regionally with large coverage.

Atmos. Chem. Phys. Discuss., doi:10.5194/acp-2016-862, 2016
Manuscript under review for journal Atmos. Chem. Phys.
Published: 30 September 2016

Atmospheric Chemistry and Physics Discussions

5 Data Availability

All data is publically archived at the NSF ACADIS website (http://articdata.io) under citation: David Sayres. 2014. Collaborative Research: Multi-Regional Scale Aircraft Observations of Methane and Carbon Dioxide Isotopic Fluxes in the Arctic. NSF Arctic Data Center. urn:uuid:58bddf69-74fe-4a20-958e-4cd23bb6941f.

Acknowledgements. This work was supported by NSF Grant 1203583 and data is archived at the ACADIS website. The authors wish to gratefully acknowledge the efforts and exceptional flying of our pilot, Bernard 'Bernie' Charlemagne, without whom these data could not have been collected.

Atmos. Chem. Phys. Discuss., doi:10.5194/acp-2016-862, 2016
Manuscript under review for journal Atmos. Chem. Phys.
Published: 30 September 2016

Atmospheric Chemistry and Physics Discussions

References

Avissar, R., Holder, H. E., Abehserra, N., Bolch, M. A., Canning, P., Magalhaes, J., Walko, R. L., Novick, K., Katul, G., Prince, K., et al.: The Duke University Helicopter Observation Platform, Bulletin of the American Meteorological Society, 90, 939–954, 2009.

Bange, J., Spiess, T., and van den Kroonenberg, A.: Characteristics of the early-morning shallow convective boundary layer from Helipod Flights during STINHO-2, Theoretical and Applied Climatology, 90, 113–126, http://dx.doi.org/10.1007/s00704-006-0272-2, 10.1007/s00704-006-0272-2, 2007.

Bastviken, D., Cole, J., Pace, M., and Tranvik, L.: Methane emissions from lakes: Dependence of lake characteristics, two regional assessments, and a global estimate, Global Biogeochemical Cycles, 18, GB4009, doi:10.1029/2004GB002238, 2004.

Berger, B. W., Davis, K. J., Yi, C. X., Bakwin, P. S., and Zhao, C. L.: Long-term carbon dioxide fluxes from a very tall tower in a northern forest: Flux measurement methodology, Journal of Atmospheric and Oceanic Technology, 18, 529–542, doi:10.1175/1520-0426(2001)018<0529:LTCDFF>2.0.CO;2, 2001.

Boucher, O., Friedlingstein, P., Collins, B., and Shine, K. P.: The indirect global warming potential and global temperature change potential due to methane oxidation, Environmental Research Letters, 4, 044 007, doi:10.1088/1748-9326/4/4/044007, 2009.

Casper, P., Maberly, S. C., Hall, G. H., and Finlay, B. J.: Fluxes of methane and carbon dioxide from a small productive lake to the atmosphere, Biogeochemistry, 49, 1–19, doi:10.1023/A:1006269900174, 2000.

Chang, R. Y. . W., Miller, C. E., Dinardo, S. J., Karion, A., Sweeney, C., Daube, B. C., Henderson, J. M., Mountain, M. E., Eluszkiewicz, J., Miller, J. B., Bruhwiler, L. M. P., and Wofsy, S. C.: Methane emissions from Alaska in 2012 from CARVE airborne observations, Proceedings of the National Academy of Sciences of the United States of America, 111, 16 694–16 699, doi:10.1073/pnas.1412953111, 2014.

Crawford, T. L. and Dobosy, R. J.: A Sensitive Fast-response Probe To Measure Turbulence and Heat-flux From Any Airplane, Boundary-layer Meteorology, 59, 257–278, doi:10.1007/BF00119816, 1992.

Crawford, T. L. and Dobosy, R. J.: Pieces to a puzzle: Air-surface exchange and climate, GPS World, 8, 32–39, 1997.

Crawford, T. L., McMillen, R. T., Dobosy, R. J., and MacPherson, I.: Correcting airborne flux measurements for aircraft speed variation, Boundary-Layer Meteorology, 66, 237–245, 1993.

Crawford, T. L., Dobosy, R. J., and Dumas, E. J.: Aircraft wind measurement considering lift-induced upwash, Boundary-layer Meteorology, 80, 79–94, doi:10.1007/BF00119012, 1996.

Damm, E., Helmke, E., Thoms, S., Schauer, U., Nothig, E., Bakker, K., and Kiene, R. P.: Methane production in aerobic oligotrophic surface water in the central Arctic Ocean, Biogeosciences, 7, 1099–1108, 2010.

Engel, G. S., Drisdell, W. S., Keutsch, F. N., Moyer, E. J., and Anderson, J. G.: Ultrasensitive near-infrared integrated cavity output spectroscopy technique for detection of CO at 1.57 mu m: new sensitivity limits for absorption measurements in passive optical cavities, Applied Optics, 45, 9221–9229, 2006.

Gioli, B., Miglietta, F., De Martino, B., Hutjes, R. W. A., Dolman, H. A. J., Lindroth, A., Schumacher, M., Sanz, M. J., Manca, G., Peressotti, A., and Dumas, E. J.: Comparison between tower and aircraft-based eddy covariance fluxes in five European regions, Agricultural and Forest Meteorology, 127, 1–16, 2004.

Gioli, B., Miglietta, F., Vaccari, F. P., Zaldei, A., and De Martino, B.: The Sky Arrow ERA, an innovative airborne platform to monitor mass, momentum and energy exchange of ecosystems, Annals of Geophysics, 49, 109–116, 2006.

Gu, L., Massman, W. J., Leuning, R., Pallardy, S. G., Meyers, T., Hanson, P. J., Riggs, J. S., Hosman, K. P., and Yang, B.: The fundamental equation of eddy covariance and its application in flux measurements, Agricultural and Forest Meteorology, 152, 135–148, 2012.

Harazono, Y., Mano, M., Miyata, A., Yoshimoto, M., Zulueta, R., Vourlitis, G., Kwon, H., and Oechel, W. C.: Temporal and spatial differences of methane flux at arctic tundra in Alaska, Mem. Natl Inst. Polar Res., Spec. Issue, 59, 79–95, 2006.

Hutjes, R. W. A., Vellinga, O. S., Gioli, B., and Miglietta, F.: Dis-aggregation of airborne flux measurements using footprint analysis, Agricultural and Forest Meteorology, 150, 966–983, 2010.

Initiative, N. S. S.: North Slope Science Initiative Landcover Mapping Summary Report, Electronic, http://catalog.northslope.org/catalogs/6979-2013-nssi-landcover-for-north-slope-of-alaska, 2013.

Kinnard, C., Zdanowicz, C. M., Fisher, D. A., Isaksson, E., de Vernal, A., and Thompson, L. G.: Reconstructed changes in Arctic sea ice over the past 1,450 years, Nature, 479, 509–U231, doi:10.1038/nature10581, 2011.

Kirby, S., Dobosy, R., Williamson, D., and Dumas, E.: An aircraft-based data analysis method for discerning individual fluxes in a heterogeneous agricultural landscape, Agricultural And Forest Meteorology, 148, 481–489, 2008.

Kirschke, S., Bousquet, P., Ciais, P., Saunois, M., Canadell, J. G., Dlugokencky, E. J., Bergamaschi, P., Bergmann, D., Blake, D. R., Bruhwiler, L., Cameron-Smith, P., Castaldi, S., Chevallier, F., Feng, L., Fraser, A., Heimann, M., Hodson, E. L., Houweling, S., Josse, B., Fraser, P. J., Krummel, P. B., Lamarque, J.-F., Langenfelds, R. L., Le Quere, C., Naik, V., O'Doherty, S., Palmer, P. I., Pison, I., Plummer, D., Poulter, B., Prinn, R. G., Rigby, M., Ringeval, B., Santini, M., Schmidt, M., Shindell, D. T., Simpson, I. J., Spahni, R., Steele, L. P., Strode, S. A., Sudo, K., Szopa, S., van der Werf, G. R., Voulgarakis, A., van Weele, M., Weiss, R. F., Williams, J. E., and Zeng, G.: Three decades of global methane sources and sinks, Nature Geoscience, 6, 813–823, doi:10.1038/NGEO1955, 2013.

Kljun, N., Rotach, M., and Schmid, H.: A three-dimensional backward lagrangian footprint model for a wide range of boundary-layer stratifications, BOUNDARY-LAYER METEOROLOGY, 103, 205–226, doi:10.1023/A:1014556300021, 2002.

Kljun, N., Calanca, P., Rotach, M., and Schmid, H.: A simple parameterisation for flux footprint predictions, BOUNDARY-LAYER METEOROLOGY, 112, 503–523, doi:10.1023/B:BOUN.0000030653.71031.96, 2004.

Koven, C. D., Ringeval, B., Friedlingstein, P., Ciais, P., Cadule, P., Khvorostyanov, D., Krinner, G., and Tarnocai, C.: Permafrost carbon-climate feedbacks accelerate global warming, Proceedings of the National Academy of Sciences of the United States of America, 108, 14 769–14 774, doi:10.1073/pnas.1103910108, 2011.

LeMone, M. A., Grossman, R. L., Chen, F., Ikeda, K., and Yates, D.: Choosing the averaging interval for comparison of observed and modeled fluxes along aircraft transects over a heterogeneous surface, Journal of Hydrometeorology, 4, 179–195, doi:10.1175/1525-7541(2003)4<179:CTAIFC>2.0.CO;2, 2003.

Mahrt, L.: Flux sampling errors for aircraft and towers, Journal Of Atmospheric And Oceanic Technology, 15, 416–429, 1998.

Metzger, S., Junkermann, W., Mauder, M., Butterbach-Bahl, K., Trancón y Widemann, B., Neidl, F., Schäfer, K., Wieneke, S., Zheng, X., Schmid, H., et al.: Spatially explicit regionalization of airborne flux measurements using environmental response functions, Biogeosciences, 10, 2193–2217, 2013.

Oechel, W. C., Vourlitis, G. L., Brooks, S., Crawford, T. L., and Dumas, E.: Intercomparison among chamber, tower, and aircraft net CO2 and energy fluxes measured during the Arctic System Science Land-Atmosphere-Ice Interactions (ARCSS-LAII) Flux Study, Journal of Geophysical Research: Atmospheres, 103, 28 993–29 003, 1998.

Oechel, W. C., Vourlitis, G. L., Verfaillie, J., Crawford, T., Brooks, S., Dumas, E., Hope, A., Stow, D., Boynton, B., Nosov, V., et al.: A scaling approach for quantifying the net CO2 flux of the Kuparuk River Basin, Alaska, Global Change Biology, 6, 160–173, 2000.

Olefeldt, D., Turetsky, M. R., Crill, P. M., and McGuire, A. D.: Environmental and physical controls on northern terrestrial methane emissions across permafrost zones, Global Change Biology, 19, 589–603, doi:10.1111/gcb.12071, 2013.

Paul, J., Lapson, L., and Anderson, J.: Ultrasensitive absorption spectroscopy with a high-finesse optical cavity and off-axis alignment, Applied Optics, 40, 4904 – 4910, 2001.

Reagan, M. T., Moridis, G. J., Elliott, S. M., and Maltrud, M.: Contribution of oceanic gas hydrate dissociation to the formation of Arctic Ocean methane plumes, Journal of Geophysical Research-oceans, 116, C09 014, doi:10.1029/2011JC007189, 2011.

Sayres, D. S., Moyer, E. J., Hanisco, T. F., Clair, J. M., Keutsch, F. N., O'Brien, A., Allen, N. T., Lapson, L., Demusz, J. N., Rivero, M., Martin, T., Greenberg, M., Tuozzolo, C., Engel, G. S., Kroll, J. H., Paul, J. B., and Anderson, J. G.: A new cavity based absorption instrument for detection of water isotopologues in the upper troposphere and lower stratosphere, Review Of Scientific Instruments, 80, 2009.

Schuur, E. A. G., McGuire, A. D., Schaedel, C., Grosse, G., Harden, J. W., Hayes, D. J., Hugelius, G., Koven, C. D., Kuhry, P., Lawrence, D. M., Natali, S. M., Olefeldt, D., Romanovsky, V. E., Schaefer, K., Turetsky, M. R., Treat, C. C., and Vonk, J. E.: Climate change and the permafrost carbon feedback, Nature, 520, 171–179, doi:10.1038/nature14338, 2015.

Sepulveda-Jauregui, A., Anthony, K. M. W., Martinez-Cruz, K., Greene, S., and Thalasso, F.: Methane and carbon dioxide emissions from 40 lakes along a north-south latitudinal transect in Alaska, Biogeosciences, 12, 3197–3223, doi:10.5194/bg-12-3197-2015, 2015.

Shakhova, N., Semiletov, I., Leifer, I., Sergienko, V., Salyuk, A., Kosmach, D., Chernykh, D., Stubbs, C., Nicolsky, D., Tumskoy, V., and Gustafsson, O.: Ebullition and storm-induced methane release from the East Siberian Arctic Shelf, Nature Geoscience, 7, 64–70, doi:10.1038/NGEO2007, 2014.

Sturtevant, C. S. and Oechel, W. C.: Spatial variation in landscape-level CO2 and CH4 fluxes from arctic coastal tundra: influence from vegetation, wetness, and the thaw lake cycle, Global Change Biology, 19, 2853–2866, doi:10.1111/gcb.12247, 2013.

Sturtevant, C. S., Oechel, W. C., Zona, D., Kim, Y., and Emerson, C. E.: Soil moisture control over autumn season methane flux, Arctic Coastal Plain of Alaska, Biogeosciences, 9, 1423–1440, doi:10.5194/bg-9-1423-2012, 2012.

Tarnocai, C., Canadell, J. G., Schuur, E. A. G., Kuhry, P., Mazhitova, G., and Zimov, S.: Soil organic carbon pools in the northern circumpolar permafrost region, Global Biogeochemical Cycles, 23, GB2023, doi:10.1029/2008GB003327, 2009.

Vellinga, O. S., Gioli, B., Elbers, J. A., Holtslag, A. A. M., Kabat, P., and Hutjes, R. W. A.: Regional carbon dioxide and energy fluxes from airborne observations using flight-path segmentation based on landscape characteristics, Biogeosciences, 7, 1307–1321, http://www.biogeosciences.net/7/1307/2010/, 2010.

Walter, K. M., Edwards, M. E., Grosse, G., Zimov, S. A., and Chapin, F. S.: Thermokarst lakes as a source of atmospheric CH4 during the last deglaciation, Science, 318, 633–636, 2007a.

Walter, K. M., Smith, L. C., and Chapin, F. S.: Methane bubbling from northern lakes: present and future contributions to the global methane budget, Philosophical Transactions of the Royal Society A-mathematical Physical and Engineering Sciences, 365, 1657–1676, 2007b.

Webb, E. K., Pearman, G. I., and Leuning, R.: Correction of Flux Measurements For Density Effects Due To Heat and Water-vapor Transfer, Quarterly Journal of the Royal Meteorological Society, 106, 85–100, doi:10.1002/qj.49710644707, 1980.

Whiticar, M. and Schaefer, H.: Constraining past global tropospheric methane budgets with carbon and hydrogen isotope ratios in ice, Philosophical Transactions of the Royal Society A-mathematical Physical and Engineering Sciences, 365, 1793–1828, doi:10.1098/rsta.2007.2048, 2007.

Witinski, M. F., Sayres, D. S., and Anderson, J. G.: High precision methane isotopologue ratio measurements at ambient mixing ratios using integrated cavity output spectroscopy, Applied Physics B-lasers and Optics, 102, 375–380, doi:10.1007/s00340-010-3957-2, 2011.

Atmos. Chem. Phys. Discuss., doi:10.5194/acp-2016-862, 2016
Manuscript under review for journal Atmos. Chem. Phys.
Published: 30 September 2016

Figure 1. Picture of the FOCAL system flying near the NOAA/ATDD flux tower in North Slope, AK.

Table 1. Flights used in the analysis along with location, time of day, mean air temperature, and surface land classes.

Flight Date YYMMDD.#	Location	Start Time UTC-10	End Time UTC-10	Temperature[1] (°C)	Dominant Land Types[2]
130813.2	Tower	08:19	10:22	16	Sedge, Mesic Sedge, Lakes, Sag river, FWM
130825.1	Tower	17:43	19:49	5	Sedge, Mesic Sedge, Lakes, Sag river, FWM
130827.1	Western Grid	09:40	13:00	6	Sedge, FWM, Lakes, Tussock tundra
130827.2	Tower	16:46	20:02	10	Sedge, Mesic Sedge, Lakes, Sag river, FWM
130828.3	Western Grid	08:39	11:39	11	Tussock tundra, Lakes, Lake margins are FWM and Sedge
130828.4	Eastern Grid	13:59	15:44	16	Sedge, Mesic Sedge, Lakes, River, FWM

[1]Temperature calculated as mean temperature recorded by instrument during flight time and below 100 m. [2]Land classes are given in order of largest percent coverage first.

Wofsy, S. C.: HIAPER Pole-to-Pole Observations (HIPPO): fine-grained, global-scale measurements of climatically important atmospheric gases and aerosols, Philosophical Transactions of the Royal Society A-mathematical Physical and Engineering Sciences, 369, 2073–2086, doi:10.1098/rsta.2010.0313, 2011.

Yvon-Durocher, G., Allen, A. P., Bastviken, D., Conrad, R., Gudasz, C., St-Pierre, A., Thanh-Duc, N., and del Giorgio, P. A.: Methane fluxes show consistent temperature dependence across microbial to ecosystem scales, Nature, 507, 488–491, doi:10.1038/nature13164, 2014.

Zachos, J. C., Dickens, G. R., and Zeebe, R. E.: An early Cenozoic perspective on greenhouse warming and carbon-cycle dynamics, Nature, 451, 279–283, doi:10.1038/nature06588, 2008.

Zulueta, R. C., Oechel, W. C., Loescher, H. W., Lawrence, W. T., and Paw U, K. T.: Aircraft-derived regional scale CO2 fluxes from vegetated drained thaw-lake basins and interstitial tundra on the Arctic Coastal Plain of Alaska, Global Change Biology, 17, 2781–2802, doi:10.1111/j.1365-2486.2011.02433.x, 2011.

Atmos. Chem. Phys. Discuss., doi:10.5194/acp-2016-862, 2016
Manuscript under review for journal Atmos. Chem. Phys.
Published: 30 September 2016

Atmospheric Chemistry and Physics Discussions

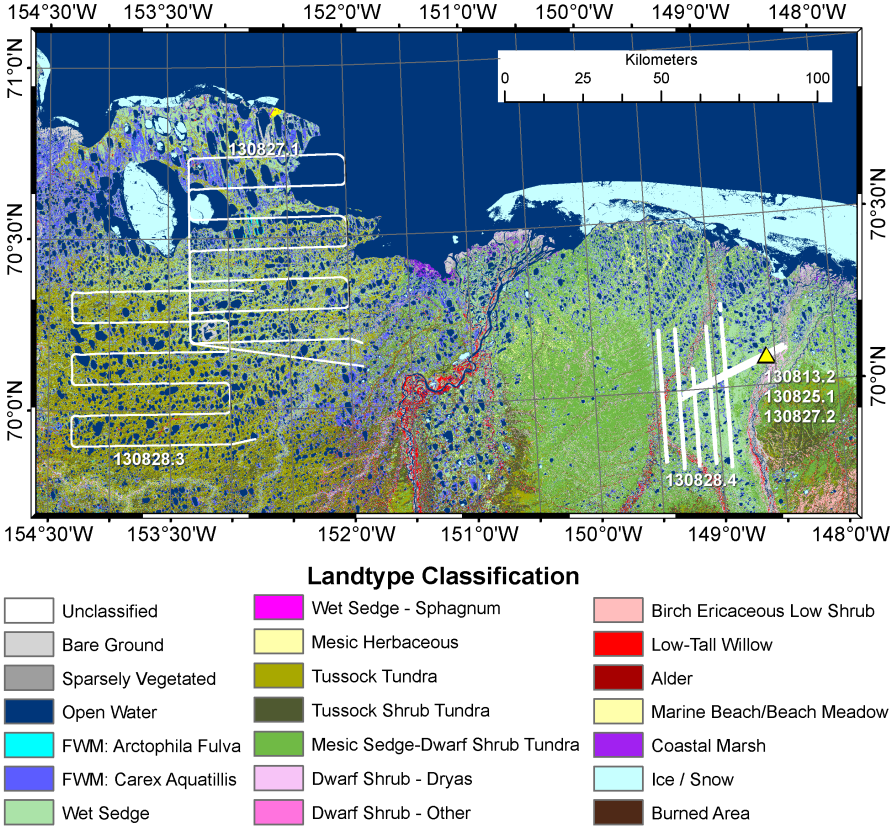

Figure 2. Six flight tracks flown by FOCAL during August, 2013 are shown in white. Dates given in the figure as YYMMDD.#, where # stands for the flight number for that day. Flight tracks shown are only for portions of the flight below 25 m above ground. Flight tracks are displayed over a false color, land cover map produced from LandSat 30 m Thematic mapper data with land types assigned by the NSSI as described in the text. Yellow triangle gives position of the NOAA/ATDD flux tower.

Atmos. Chem. Phys. Discuss., doi:10.5194/acp-2016-862, 2016
Manuscript under review for journal Atmos. Chem. Phys.
Published: 30 September 2016

Atmospheric Chemistry and Physics Discussions

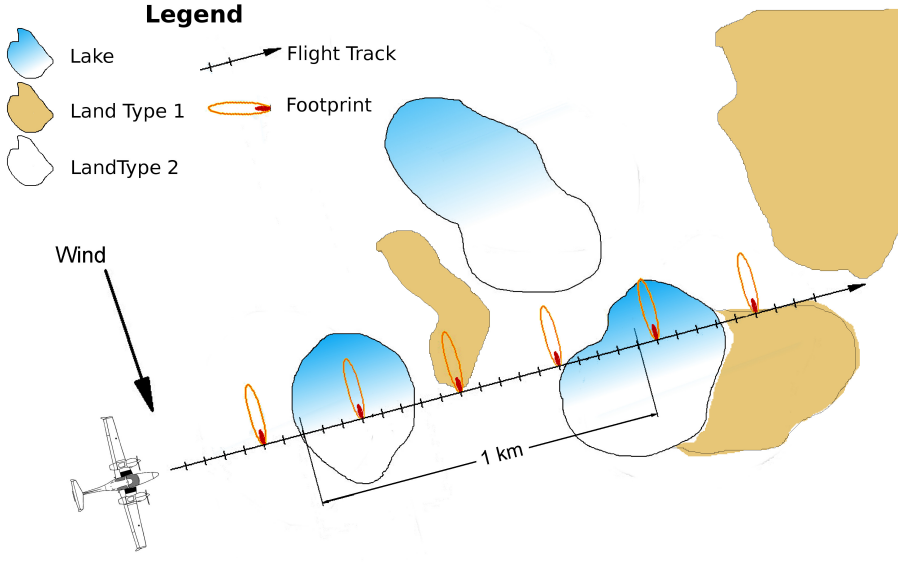

Figure 3. The Flux Fragment Method (FFM) relies on dividing up the covariance measurements into small fragments whose footprints can be attributed to different landscape features or classes. In the figure the landscape has been divided into lakes and two types of land, for example wet sedge and fresh water marsh. Footprints are calculated for each fragment and footprints that lie mostly (>85%) on a single land type are labeled as that land type. All footprints for a single land type can then be summed and divided by the cumulative path length in air.

Atmos. Chem. Phys. Discuss., doi:10.5194/acp-2016-862, 2016
Manuscript under review for journal Atmos. Chem. Phys.
Published: 30 September 2016

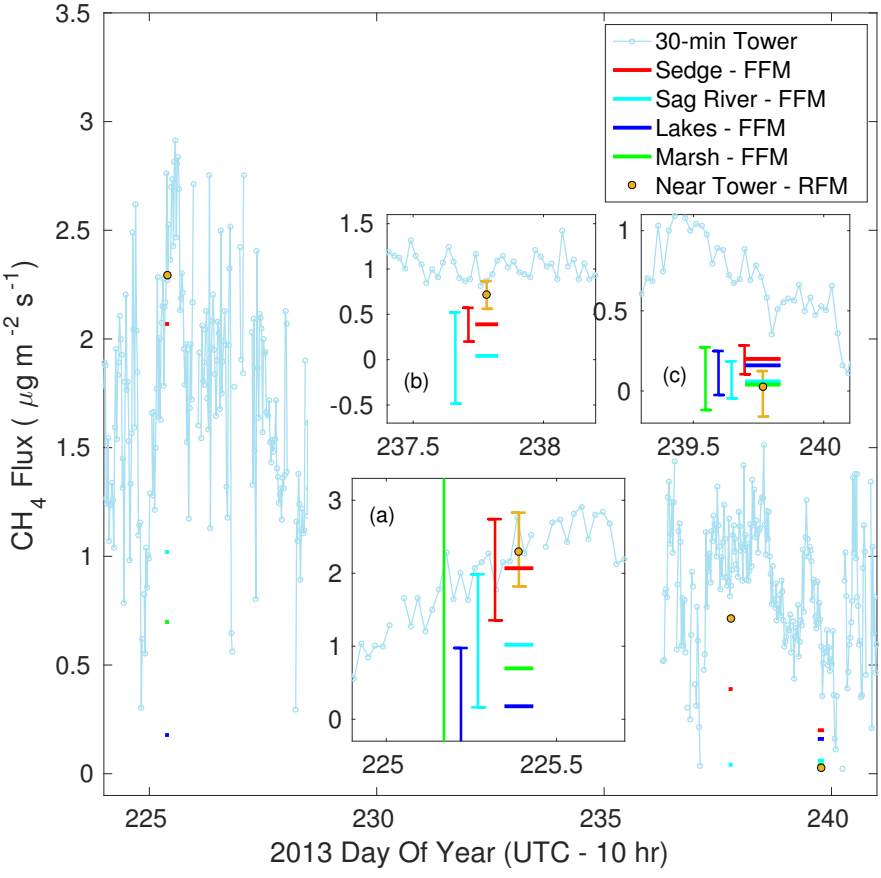

Figure 4. Comparison of methane flux measured by the flux tower with fluxes measured by the FOCAL system. Tower methane fluxes are 30-minute means plotted versus day of year. Three flights (Aug. 13, 25, and 27) made repeated flight transects near the tower. A running mean flux using the nearest 3 km of flight track to the tower for each leg was calculated and the mean of these fluxes is plotted for each day as an orange circle. Fluxes for sedge, marsh, lakes, and the Sag river were calculated using FFM using data from the whole flight and are plotted for each day, color coded according to the legend, with the length of the line along the time axis representing the time over which the data were taken. Insets (a), (b), and (c) show details for each flight day with bars showing the 95% confidence interval based on bootstrap analysis. Bars are offset along the x-axis for clarity.

Atmos. Chem. Phys. Discuss., doi:10.5194/acp-2016-862, 2016
Manuscript under review for journal Atmos. Chem. Phys.
Published: 30 September 2016

Atmospheric Chemistry and Physics Discussions

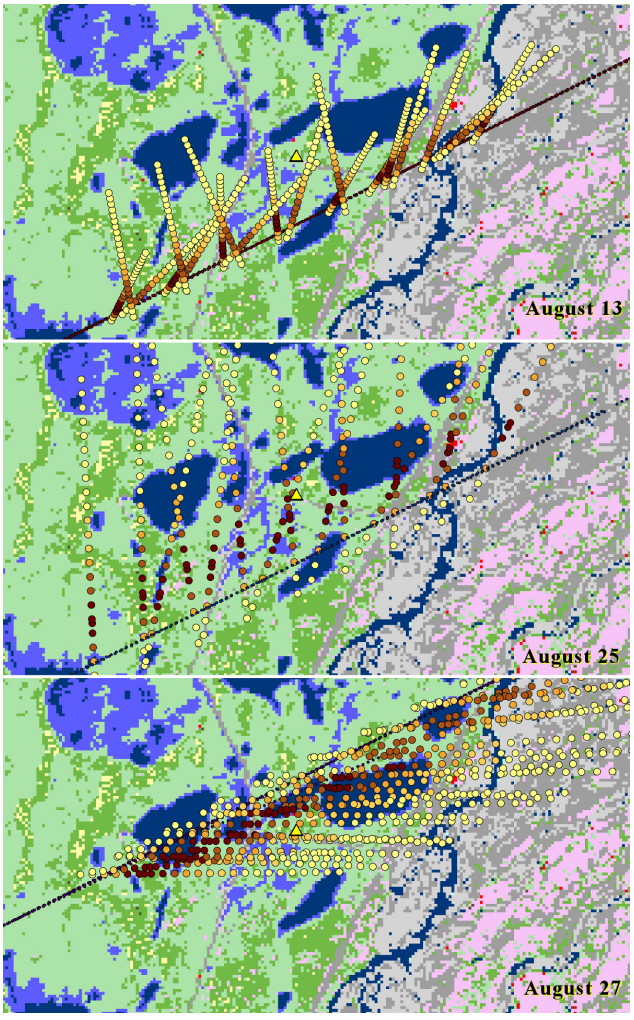

Figure 5. Map of area surrounding the flux tower (yellow triangle) with false color map representing different land classes defined as in Fig. 2. The flight track for each flight is shown as black points, where each point is the start position of a flux fragment. Flux footprints for selected fragments are shown as colored dots with darker and redder dots representing larger probability of contribution to the total flux as described in the text.

Atmos. Chem. Phys. Discuss., doi:10.5194/acp-2016-862, 2016
Manuscript under review for journal Atmos. Chem. Phys.
Published: 30 September 2016

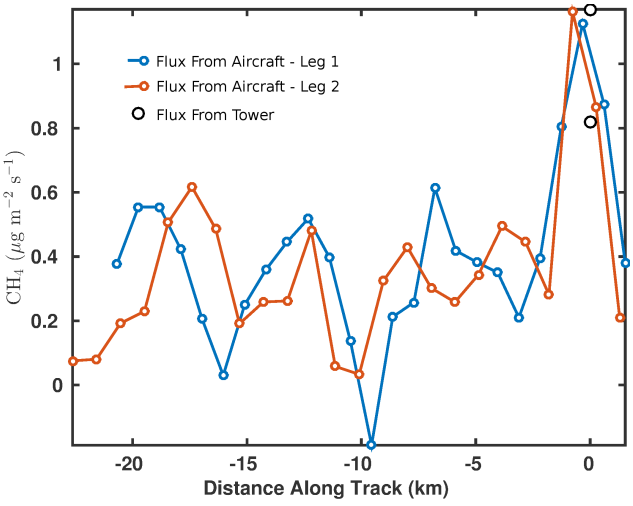

Figure 6. Plot of methane flux derived using RFM versus distance from flux tower for two flight legs on August 25. Positive (negative) distance is East (West) of the tower position. The East to West transect (blue) was flown 30 minutes after the West to East transect (orange). Black circles are the methane flux measured by the tower at the nearest time to when the aircraft passed the tower.

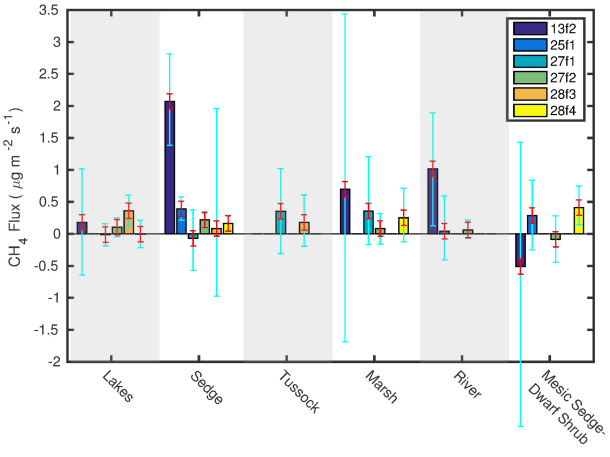

Figure 7. Methane fluxes by land surface class derived using the FFM for each of six flights as given in the legend. Dates of flights are given as day of month in August followed by the flight number for that day. Bars give the instrument uncertainty (red) and the 95% confidence interval as calculated using bootstrapping (blue).